UJEAS

UNIZIK JOURNAL OF ENGINEERING AND APPLIED SCIENCES

UNIZIK Journal of Engineering and Applied Sciences 6(4), December (2026), 4079-4093
Journal homepage: https://journals.unizik.edu.ng/index.php/ujeas
PRINT ISSN: 2992-4383 || ONLINE ISSN: 2992-4391

Voltage Stability Assessment of a Grid-Connected Wind Turbine on the BEDC Network Using Newton–Raphson Load Flow Analysis

Efetobor Mathew Ufuoma[1], Anazia Emmanuel Aninye[2], Aghara Jachimma Vincent [3], Ibeh Charles Austeen[4], Anionovo Ugochukwu Edebeani[5]

[1]Dieu Engineering ltd
[2,3,5]Deparment of Electrical Engineering, Nnamdi Azikiwe University, Awka.
[4]Forensic Science Department, Nnamdi Azikiwe University, Awka.
Corresponding Author's Email: ue.anionovo@unizik.edu.ng

Abstract
This study evaluates the voltage stability of a grid-connected wind turbine integrated into the Benin Electricity Distribution Company (BEDC) network using Newton–Raphson load flow and transient simulations in PowerWorld Simulator. The network was analyzed under steady-state and three-phase fault conditions before and after wind turbine integration. A three-phase fault was applied to Feeder II of the Amukpe 132/33 kV substation. Results showed improved voltage stability following wind turbine integration. The minimum voltage increased from 0.2981 p.u. to 0.31153 p.u., while stabilization time decreased from approximately 4.7503 s to 2.191762 s. In addition, the maximum voltage angle reduced from 6.32887° to 2.53556°, with fewer system oscillations observed. These findings indicate that wind energy integration can improve transient voltage response, enhance damping, and strengthen the overall stability and reliability of the BEDC network.
Keywords: Voltage Stability, Wind Energy, BEDC Network, Newton–Raphson Method, PowerWorld Simulator, Renewable Energy Integration, Transient Stability.

1. Introduction

Electricity remains one of the most important drivers of economic growth and industrial development. The Nigerian power sector continues to experience inadequate generation capacity, voltage instability, and frequent grid collapses due to aging infrastructure and insufficient generation reserves. Despite having an installed generation capacity that exceeds 5 GW, the average available power generation remains significantly below national demand.

The increasing need for sustainable and reliable power supply has encouraged the integration of renewable energy sources into conventional power systems. In Nigeria, the transition toward a more diversified renewable-energy mix has been identified as an important pathway for improving long-term energy security (Akuru et al., 2017). Among the available renewable energy sources, wind energy is particularly attractive because of its environmental benefits, low operating emissions, and scalability. Nevertheless, high levels of wind penetration can alter conventional power-system dynamics, making voltage regulation, inertia, and transient stability increasingly important considerations (Flynn et al., 2017).

However, integrating wind energy into weak power networks such as the BEDC network introduces several technical challenges related to voltage regulation, reactive power compensation, and transient stability. Therefore, there is a need to investigate the effects of wind turbine integration on the voltage stability performance of the BEDC network.

This paper evaluates the impact of integrating a wind turbine into the BEDC network under normal and fault conditions using Newton–Raphson load flow analysis and transient simulation techniques.
Several studies have investigated the influence of wind-energy integration on power-system voltage stability. Malik et al. (2024) reviewed voltage-stability issues in wind-integrated power systems and identified reduced system strength, reactive-power imbalance, and converter interactions as important causes of instability. Adetokun et al. (2020) assessed increasing DFIG-based wind penetration and showed that voltage-stability margins can deteriorate as penetration rises unless network reinforcement or reactive-power compensation is provided.
Transient-stability studies have similarly shown that the dynamic effect of wind generation depends strongly on wind-farm location, penetration level, turbine control, and reactive-power support. Xia et al. (2018) demonstrated that wind-

farm capacity, siting, and wind speed can significantly influence transient response, while Tina et al. (2022) compared technical measures such as SVC, STATCOM, fast excitation, and transmission reinforcement for improving transient stability in wind-integrated systems. Hu et al. (2022) examined direct-drive wind turbines during grid faults and highlighted the importance of DC-link voltage dynamics during fault recovery. More recently, Shabani et al. (2023) showed that reactive-power control and wind-turbine drivetrain characteristics can materially affect the transient stability of DFIG-based wind-farm systems.

For the Nigerian grid, Adetokun and Muriithi (2021) demonstrated that large-scale DFIG-based wind integration can improve the voltage profile and voltage-stability margin of a weak 330 kV network when an appropriate penetration level is selected. Verma et al. (2023) further emphasized that converter-dominated wind systems can introduce oscillatory interactions that require adequate damping and control. Despite these advances, relatively few studies have examined the transient voltage response of Nigerian distribution networks, particularly the BEDC network, under severe three-phase disturbances. This study addresses that gap by comparing the BEDC network before and after wind-turbine integration Electricity remains one of the most important drivers of economic growth and industrial development. The Nigerian power sector continues to experience inadequate generation capacity, voltage instability, and frequent grid collapses due to aging infrastructure and insufficient generation reserves. Despite having an installed generation capacity that exceeds 5 GW, the average available power generation remains significantly below national demand.

The increasing need for sustainable and reliable power supply has encouraged the integration of renewable energy sources into conventional power systems. In Nigeria, the transition toward a more diversified renewable-energy mix has been identified as an important pathway for improving long-term energy security (Akuru et al., 2017). Among the available renewable energy sources, wind energy is particularly attractive because of its environmental benefits, low operating emissions, and scalability. Nevertheless, high levels of wind penetration can alter conventional power-system dynamics, making voltage regulation, inertia, and transient stability increasingly important considerations (Flynn et al., 2017).
However, integrating wind energy into weak power networks such as the BEDC network introduces several technical challenges related to voltage regulation, reactive power compensation, and transient stability. Therefore, there is a need to investigate the effects of wind turbine integration on the voltage stability performance of the BEDC network. This paper evaluates the impact of integrating a wind turbine into the BEDC network under normal and fault conditions using Newton–Raphson load flow analysis and transient simulation techniques.
Several studies have investigated the influence of wind-energy integration on power-system voltage stability. Malik et al. (2024) reviewed voltage-stability issues in wind-integrated power systems and identified reduced system strength, reactive-power imbalance, and converter interactions as important causes of instability. Adetokun et al. (2020) assessed increasing DFIG-based wind penetration and showed that voltage-stability margins can deteriorate as penetration rises unless network reinforcement or reactive-power compensation is provided.

Transient-stability studies have similarly shown that the dynamic effect of wind generation depends strongly on wind-farm location, penetration level, turbine control, and reactive-power support. Xia et al. (2018) demonstrated that wind-farm capacity, siting, and wind speed can significantly influence transient response, while Tina et al. (2022) compared technical measures such as SVC, STATCOM, fast excitation, and transmission reinforcement for improving transient stability in wind-integrated systems. Hu et al. (2022) examined direct-drive wind turbines during grid faults and highlighted the importance of DC-link voltage dynamics during fault recovery. More recently, Shabani et al. (2023) showed that reactive-power control and wind-turbine drivetrain characteristics can materially affect the transient stability of DFIG-based wind-farm systems.

For the Nigerian grid, Adetokun and Muriithi (2021) demonstrated that large-scale DFIG-based wind integration can improve the voltage profile and voltage-stability margin of a weak 330 kV network when an appropriate penetration level is selected. Verma et al. (2023) further emphasized that converter-dominated wind systems can introduce oscillatory interactions that require adequate damping and control. Despite these advances, relatively few studies have examined the transient voltage response of Nigerian distribution networks, particularly the BEDC network, under severe three-phase disturbances. This study addresses that gap by comparing the BEDC network before and after wind-turbine integration using Newton-Raphson load-flow analysis and time-domain transient simulation, with emphasis on voltage magnitude, voltage-angle oscillation, and post-fault stabilization time.using Newton-Raphson load-flow analysis and time-domain transient simulation, with emphasis on voltage magnitude, voltage-angle oscillation, and post-fault stabilization time.

2.0 Materials and methods

2.1 System Description

The BEDC network was modeled using PowerWorld Simulator based on actual network parameters obtained from the distribution company. The modeled network includes transmission lines, transformers, buses, and distribution feeders operating at 132/33 kV as shown in figure 1. Figure 2 shows when the wind turbine was integrated. Tables 1, 2, and 3 shows the network parameters before simulation.

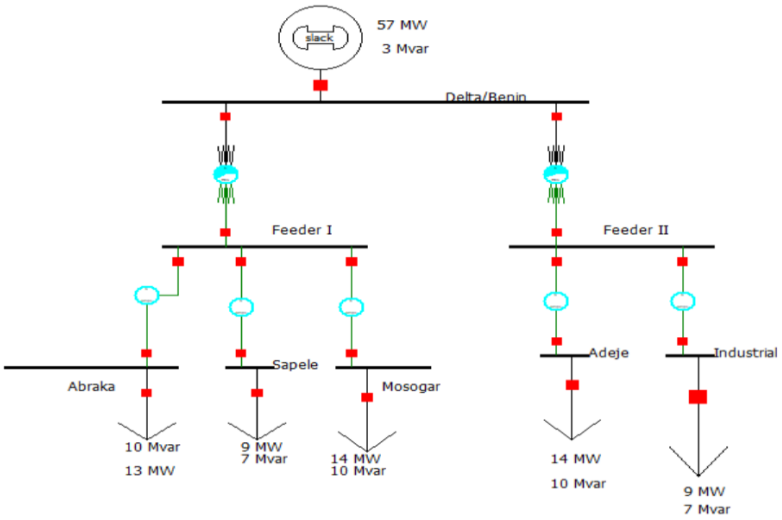

Figure 1: base network modeled in PowerWorld.

Table 1: initial bus parameters before load flow simulation

Number	Name	Nom kV	PU Volt	Volt (kV)	Angle (Deg)	Load MW	Load Mvar	Gen MW	Gen Mvar
1	Delta/Benin	132	1.025	135.3	0			0	0
2	Feeder I	33	1	33.655	0				
3	Feeder II	33	1	33.935	0				
4	Abraka	33	1	33.246	0	13.4	10.3		
5	Sapele	33	1	33.613	0	9.2	6.9		
6	Mosogar	33	1	33.64	0	13.7	10.3		
7	Adeje	33	1	33.672	0	13.7	10.3		
8	Industrial	33	1	33.511	0	9.15	6.86		

Table 2: The distribution line parameters before load flow simulation

From Name	To Name	Status	Branch Device Type	Xfrmr	R	X	B	Lim MVA A
Delta/Benin	Feeder I	Closed	Transformer	YES	0	0.125	0	60
Delta/Benin	Feeder II	Closed	Transformer	YES	0	0.124	0	40
Feeder I	Abraka	Closed	Line	NO	0.03676	0.07404	0.00209	0
Feeder I	Sapele	Closed	Line	NO	0.34596	0.58032	0.0007	0
Feeder I	Mosogar	Closed	Line	NO	0.45048	0.86428	0.00175	0
Feeder II	Adeje	Closed	Line	NO	0.25948	0.43525	0.00052	0
Feeder II	Industrial	Closed	Line	NO	0.34596	0.58032	0.0007	0

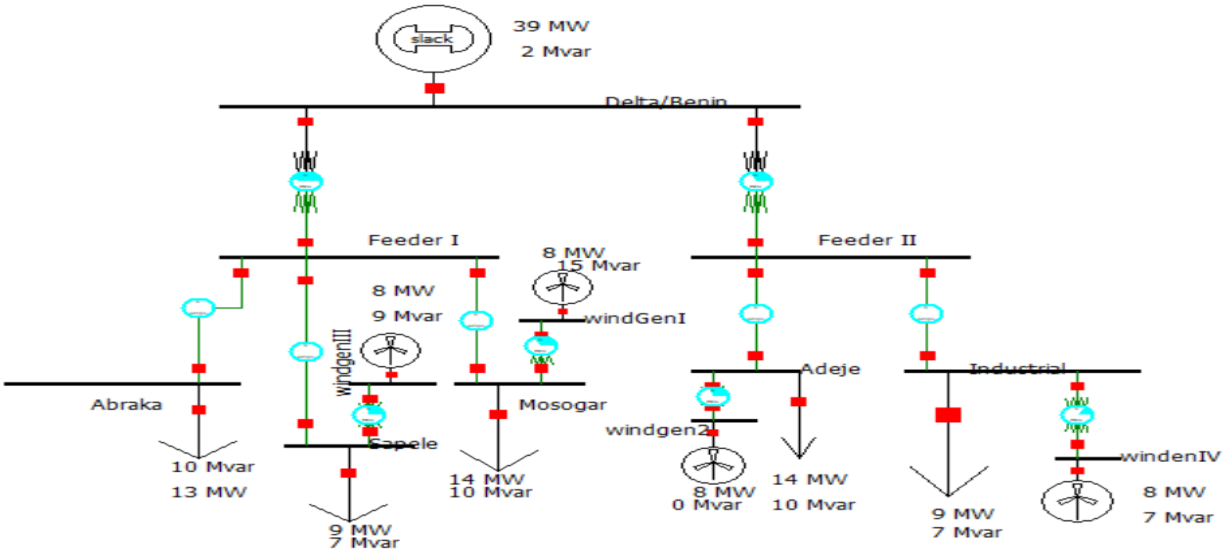

Figure 2: integration of wind turbine to the network.

Table 3: showing the parameters of wind turbine generator

S/N	Parameter	Specification
1	Wind-generator model	Variable-speed Type 3 DFIG
2	Number of equivalent units	4
3	Rated power per unit	7.88 MW
4	Total installed capacity	31.52 MW
5	Stator resistance, (R_s)	0.00707 pu
6	Stator inductance, (L_s)	0.171 pu
7	Rotor resistance, (R_r)	0.005 pu
8	Rotor inductance, (L_r)	0.156 pu
9	Magnetising inductance, (L_m)	2.9 pu
10	Power coefficient, (C_p)	0.3012
11	Air density, (\rho)	1.225 kg/m³
12	Number of poles	4
13	Gearbox ratio	0.103472222
14	Blade length/rotor radius	75 m
15	Number of blades	3
16	System frequency	50 Hz
17	Generator terminal voltage	4 kV AC
18	Step-up transformer ratio	4/33 kV

2.2 Load Flow Analysis

2.2.1 Newton–Raphson Load Flow Equations

Consider an *n*-bus power system represented by its bus admittance matrix. The injected complex power at bus *i* is expressed as

$$S_i = P_i + jQ_i \quad (1)$$

where

P_i= Active power injected at bus *i*

Q_i= Reactive power injected at bus *i*

The complex power is related to the bus voltage and injected current by

$$S_i = V_i I_i^* \quad (2)$$

The injected current at bus *i* is expressed as

$$I_i = \sum_{j=1}^{n} Y_{ij} V_j \tag{3}$$

Substituting the current equation into the power equation gives

$$S_i = V_i \left(\sum_{j=1}^{n} Y_{ij} V_j \right)^* \tag{4}$$

Expressing the bus voltages and admittances in polar form yields the active and reactive power equations.
The active power at bus *i* is given by

$$P_i = \sum_{j=1}^{n} | V_i | | V_j | | Y_{ij} | \cos(\theta_{ij} + \delta_j - \delta_i) \tag{5}$$

while the reactive power is

$$Q_i = -\sum_{j=1}^{n} | V_i | | V_j | | Y_{ij} | \sin(\theta_{ij} + \delta_j - \delta_i) \tag{6}$$

where

1. V_i, V_j are bus voltage magnitudes,
2. δ_i, δ_j are voltage angles,
3. Y_{ij} is the element of the bus admittance matrix,
4. θ_{ij} is the admittance angle.

These nonlinear equations are solved iteratively using the Newton–Raphson algorithm until the specified convergence tolerance is achieved.

2.2.2 Bus Admittance Matrix (Y-Bus)

The bus admittance matrix is the mathematical representation of the electrical connections between buses in a power network. It contains the self-admittance and mutual admittance of all buses and forms the basis of load flow calculations.
The Y-Bus matrix is expressed as

$$Y_{Bus} = \begin{bmatrix} Y_{11} & Y_{12} & \cdots & Y_{1n} \\ Y_{21} & Y_{22} & \cdots & Y_{2n} \\ \vdots & \vdots & \ddots & \vdots \\ Y_{n1} & Y_{n2} & \cdots & Y_{nn} \end{bmatrix} \tag{7}$$

The off-diagonal elements are

$$Y_{ij} = -y_{ij} \tag{8}$$

where y_{ij} is the admittance of the transmission line connecting buses *i* and *j*.
The diagonal elements are

$$Y_{ii} = \sum_{j=1}^{n} y_{ij} + y_{sh} \tag{9}$$

where

- y_{ij} = transmission line admittance,
- y_{sh} = shunt admittance connected to the bus.

The admittance itself is represented as

$$Y = G + jB \tag{10}$$

where

1. G = conductance,
2. B = susceptance.

3.2.3 Power Mismatch Equations

During each iteration, the scheduled power is compared with the calculated power to determine the power mismatch.
The active power mismatch is

$$\Delta P_i = P_i^{spec} - P_i^{calc} \tag{12}$$

The reactive power mismatch is

$$\Delta Q_i = Q_i^{spec} - Q_i^{calc} \tag{13}$$

The Newton–Raphson method updates the voltage magnitude and voltage angle using the Jacobian matrix according to

$$\begin{bmatrix} \Delta P \\ \Delta Q \end{bmatrix} = J \begin{bmatrix} \Delta \delta \\ \Delta V \end{bmatrix} \tag{14}$$

where

- J = Jacobian matrix,
- $\Delta\delta$ = correction in voltage angles,
- ΔV = correction in voltage magnitudes.

The Jacobian matrix consists of four sub-matrices

$$J = \begin{bmatrix} J_1 & J_2 \\ J_3 & J_4 \end{bmatrix} \quad (13)$$

representing the partial derivatives of active and reactive power with respect to voltage angles and voltage magnitudes. The iterative process continues until

$\max(|, \Delta P \; || \; \Delta Q \; |) \leq \varepsilon$

where $\varepsilon$is the specified convergence tolerance.

2.3 Fault Analysis

A balanced three-phase fault was applied on Feeder II of the Amukpe 132/33 kV substation to evaluate the transient stability performance of the BEDC network.

For a three-phase fault, only the positive sequence network is considered, and the fault current is expressed as:

$$I_{a1} = \frac{1.0\angle 0^\circ}{Z_1 + Z_f} \quad (14)$$

For a solid fault where the fault impedance is negligible:

$$I_{a1} = \frac{1.0\angle 0^\circ}{Z_1} \quad (15)$$

The phase currents are given by:

$$I_{af} = I_{a1}, I_{bf} = a^2 I_{a1}, I_{cf} = a I_{a1} \quad (16)$$

where:

$$a = 1\angle 120^\circ$$

The transient response of the network was evaluated using voltage angle variation, per-unit voltage response, and stabilization time after fault clearance.

2.4 Transient Stability

In this study, transient stability analysis was carried out using Power world to evaluate the dynamic response of the Amukpe 132/33 kV power network following the application of a three-phase fault. The transient behaviour of the system was assessed by monitoring the generator voltage angle, voltage response and system oscillations before and after the integration of wind turbine.

2.4.1 Swing Equation

The swing equation is the fundamental mathematical model used to describe the electromechanical dynamics of a synchronous generator during transient disturbances. It represents the relationship between the accelerating power acting on the generator rotor and its angular motion.

The swing equation is expressed as

$$M \frac{d^2\delta}{dt^2} = P_m - P_e \quad (17)$$

where:

M= angular momentum of the generator rotor (MJ/MVA)

δ= rotor angle (electrical degrees or radians)

P_m= mechanical input power (p.u.)

P_e= electrical output power (p.u.)

The difference between the mechanical and electrical powers is known as the accelerating power,

$$P_a = P_m - P_e \quad (18)$$

When $P_m > P_e$, the generator accelerates and the rotor angle increases. Conversely, when $P_m < P_e$, the generator decelerates and the rotor angle decreases. Following a disturbance, the continuous variation of the rotor angle determines whether the generator remains synchronized with the rest of the power system.

2.4.2 Power–Angle Equation

The electrical power transmitted by a synchronous generator is a function of the rotor angle between the internal generated voltage and the receiving-end voltage. This relationship is described by the power-angle equation:

$$P_e = \frac{EV}{X} \sin \delta \quad (19)$$

where:

- P_e= electrical power output
- E= internal generator voltage
- V= bus voltage
- X= equivalent transfer reactance

- δ= rotor angle

The equation shows that the transmitted electrical power increases as the rotor angle increases, reaching a maximum value when the rotor angle is approximately **90°**. Beyond this point, the transmitted power decreases, increasing the possibility of instability if the disturbance persists.

During a fault, the transfer reactance effectively increases, reducing the electrical power transferred through the network. This causes an increase in the accelerating power acting on the generator rotor. Following fault clearance, the power transfer capability is restored, allowing the generator to decelerate and regain synchronism if the fault has been cleared within the critical time.

2.4.3 Equal Area Criterion

The Equal Area Criterion is a graphical method used to determine the transient stability of a single-machine infinite-bus (SMIB) system following a disturbance. The criterion states that the system remains stable if the kinetic energy gained by the generator rotor during the fault is equal to or less than the kinetic energy dissipated after the fault is cleared.

The accelerating energy is represented by the area

$$A_1 = \int_{\delta_0}^{\delta_c} (P_m - P_e) d\delta \quad (20)$$

while the decelerating energy is

$$A_2 = \int_{\delta_c}^{\delta_m} (P_e - P_m) d\delta \quad (21)$$

where:

- δ_0= initial rotor angle
- δ_c= rotor angle at fault clearing
- δ_m= maximum rotor angle

For transient stability,

$$A_1 \leq A_2$$

When the accelerating area exceeds the decelerating area, the generator cannot regain synchronism, resulting in transient instability.

Although power world automatically performs transient stability calculations numerically, the Equal Area Criterion provides a useful theoretical basis for understanding the voltage angle behaviour observed during the simulations.

2.5 Wind Turbine Integration

The wind turbine model was connected to the BEDC network and simulations were repeated under steady-state and transient conditions. Wind speed data for Benin City was used to estimate the wind turbine operating conditions.

3. Results and Discussion

Tables 4 shows the Transient Analysis result in per-unit of voltage, with and without Wind Turbine Integration, while figure 5 shows the Transient Analysis result of voltage angle with and without Wind Turbine Integration

Table 4: Transient Analysis result for per-unit voltage with and without Wind Turbine Integration

Time (s)	Bus Sapele V pu without wind generator	Bus Sapele V pu with wind generator
1.000000	0.90263	1.01851
1.000000	0.37487	0.40505
1.154179	0.29806	0.31158
1.183348	0.29811	0.31148
1.253000	0.71899	0.78288
1.800064	0.92686	1.05041
2.175094	0.92850	1.05469
2.245933	0.92843	1.05489
2.475118	0.92728	1.05391
2.662633	0.92550	1.05167
2.862649	0.92305	1.04829
3.050164	0.92042	1.04448
3.212677	0.91799	1.04087
3.541870	0.91300	1.03328
3.741886	0.91013	1.02884
3.929401	0.90765	1.02498
4.137751	0.90520	1.02116
4.333600	0.90323	1.01810
4.529449	0.90161	1.01559
4.733632	0.90029	1.01358
4.950316	0.89928	1.01210
5.154499	0.89868	1.01127
5.367016	0.89837	1.01093
5.554531	0.89833	1.01101
5.742046	0.89847	1.01138
5.933728	0.89876	1.01199
6.108742	0.89913	1.01270
6.287923	0.89957	1.01353
6.483772	0.90011	1.01450
6.733792	0.90083	1.01576
6.929641	0.90138	1.01670
7.204663	0.90210	1.01789
7.417180	0.90259	1.01867
7.575526	0.90291	1.01916
7.754707	0.90322	1.01962
7.971391	0.90352	1.02004
8.167240	0.90373	1.02029
8.375590	0.90388	1.02044
8.588107	0.90397	1.02048
8.763121	0.90400	1.02045
8.992306	0.90399	1.02033
9.200656	0.90394	1.02016
9.434008	0.90385	1.01993
9.546517	0.90380	1.01981
9.767368	0.90368	1.01956
10.046557	0.90353	1.01926
10.250740	0.90342	1.01906

10.429921	0.90333	1.01890
10.571599	0.90326	1.01879
10.83412	0.90315	1.01862
11.092474	0.90306	1.0185
11.288323	0.90301	1.01844
11.463337	0.90297	1.01841
11.655019	0.90294	1.01839
11.850868	0.90292	1.01839
12.071719	0.90291	1.01841
12.267568	0.90291	1.01844
12.338407	0.90292	1.01846
12.559258	0.90292	1.0185
12.730105	0.90294	1.01855
12.938455	0.90295	1.01859
13.171807	0.90298	1.01865
13.484332	0.90301	1.01872
13.538503	0.90301	1.01872
13.796857	0.90304	1.01877
14.038543	0.90306	1.0188
14.3344	0.90308	1.01883
14.480245	0.90308	1.01883
14.538583	0.90309	1.01884
14.746933	0.90309	1.01885
15.00112	0.9031	1.01885
15.33448	0.9031	1.01883
15.546997	0.9031	1.01883
15.580333	0.9031	1.01882
15.784516	0.9031	1.01882
16.151212	0.9031	1.0188
16.234552	0.90309	1.01879
16.555411	0.90309	1.01878
16.576246	0.90309	1.01877
16.809598	0.90308	1.01876
17.08462	0.90308	1.01876
17.16796	0.90307	1.01875
17.567992	0.90307	1.01875
17.718004	0.90306	1.01874
17.776342	0.90306	1.01874
17.976358	0.90306	1.01874
18.37639	0.90306	1.01874
18.493066	0.90306	1.01875
18.58474	0.90306	1.01874
18.784756	0.90306	1.01875
19.059778	0.90306	1.01875
19.188955	0.90305	1.01875

19.50148	0.90305	1.01876
19.593154	0.90305	1.01875
19.797337	0.90305	1.01876
20	0.90305	1.01876

Table 5 Transient Analysis result for voltage angle with and without Wind Turbine Integration

Time (s)	V Angle Without Wind Turbine	V Angle With Wind Turbine
1.000000	-4.69451	-3.63989
1.008334	1.32006	-0.91919
1.025002	3.40247	0.40569
1.037503	4.42803	1.08763
1.054171	5.28254	1.72456
1.066672	5.66674	2.01885
1.083340	5.96539	2.25704
1.095841	6.10515	2.36265
1.108342	6.17952	2.42453
1.125010	6.24402	2.47649
1.137511	6.28266	2.50519
1.154179	6.30453	2.52299
1.179181	6.31992	2.53556
1.195849	6.32462	2.53946
1.208350	6.32658	2.53355
1.225018	6.32802	2.53464
1.237519	6.32858	2.54384
1.245853	6.32880	2.54627
1.253000	6.32892	2.53878
1.258354	0.97398	1.14081
1.262521	0.47966	0.78274
1.291690	-1.90553	-1.02605
1.325026	-3.33906	-2.21963
1.354195	-4.00352	-2.82655
1.383364	-4.36520	-3.18507
1.416700	-4.57734	-3.41414
1.445869	-4.67047	-3.52378
1.475038	-4.71952	-3.58627
1.508374	-4.74817	-3.62569
1.537543	-4.76118	-3.64497
1.566712	-4.76854	-3.65653
1.600048	-4.77337	-3.66454
1.629217	-4.77589	-3.66897
1.658386	-4.77751	-3.67201
1.691722	-4.77863	-3.67402
1.750060	-4.77944	-3.67569
1.762561	-4.77947	-3.67581
1.783396	-4.77945	-3.67596
1.804231	-4.77934	-3.67603
1.812565	-4.77927	-3.67603
1.841734	-4.77897	-3.67600
1.875070	-4.77851	-3.67587
1.904239	-4.77805	-3.67573
1.933408	-4.77756	-3.67558
1.966744	-4.77698	-3.67544
1.995913	-4.77648	-3.67467
2.000080	-4.77641	-3.67459
2.333440	-4.77164	-3.67100
2.666800	-4.76688	-3.66963

3.000160	-4.76208	-3.66851
3.333520	-4.75787	-3.66755
3.662713	-4.75454	-3.66717
3.996073	-4.75210	-3.66725
4.329433	-4.75056	-3.66730
4.662793	-4.74982	-3.66752
4.996153	-4.74971	-3.66797
5.000320	-4.74971	-3.66789
6.071239	-4.75159	-3.66864
8.213077	-4.75369	-3.66862
9.288163	-4.75291	-3.66829
10.359082	-4.75207	-3.66805
11.430001	-4.75153	-3.66800
12.500920	-4.75121	-3.66803
13.571839	-4.75092	-3.66782
14.642758	-4.75057	-3.66769
15.713677	-4.75019	-3.66764
16.788763	-4.74980	-3.66752
17.859682	-4.74942	-3.66736
18.930601	-4.74905	-3.66727
20.000000	-4.74869	-3.66724

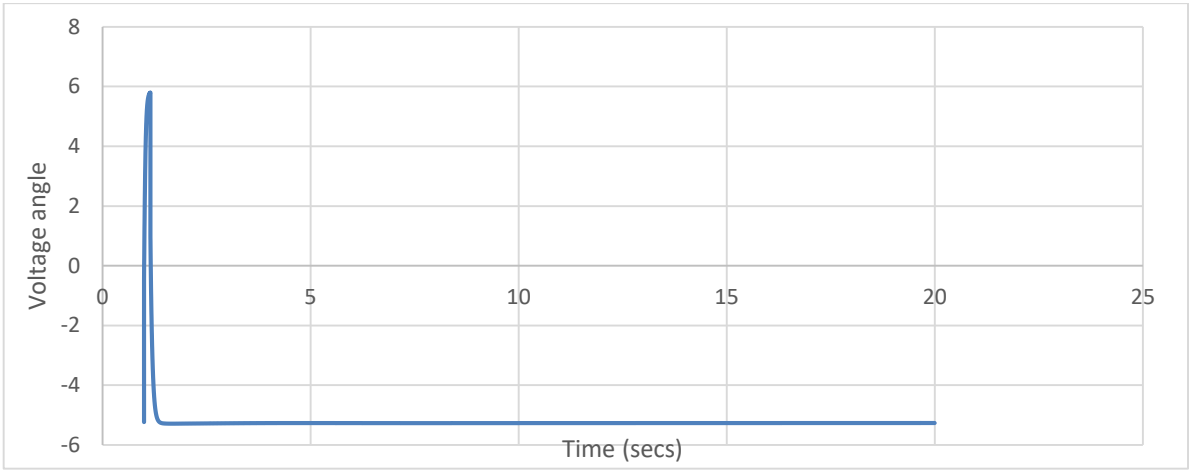

Figure 3: A plot of the voltage angle against time without the connection of the Wind Turbine

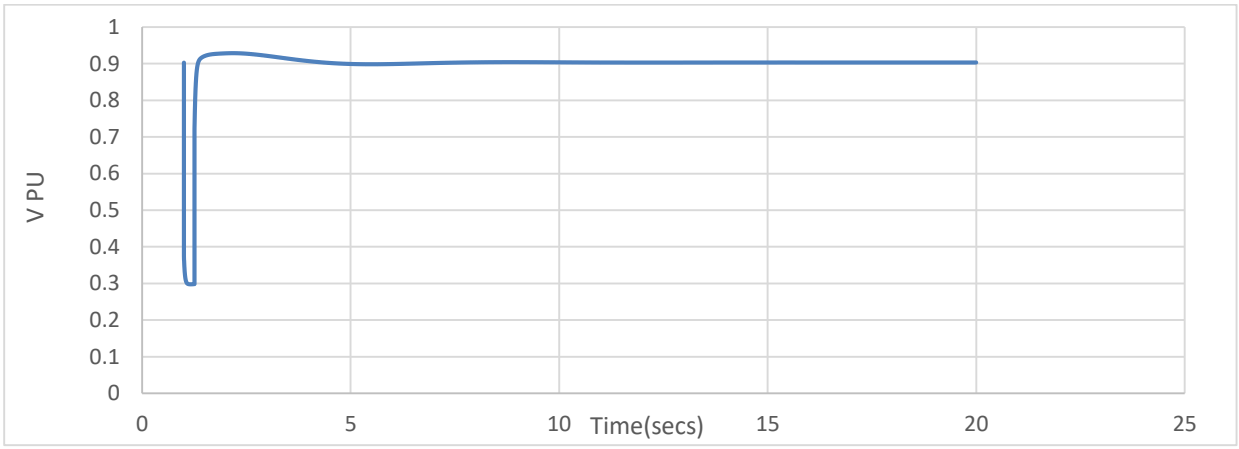

Figure 4: A plot of the per-unit Voltage against time without the connection of the Wind Turbine

The transient stability simulation under a three-phase fault condition revealed severe instability in the BEDC network before wind turbine integration.

The highest voltage angle recorded during the disturbance was 6.32887° at 1.253 seconds. The lowest voltage angle was −4.77947° at approximately 1.766728 seconds during system oscillation. The system eventually stabilized after approximately 4.7503 seconds as shown in figure 3.

Similarly, the per-unit voltage dropped significantly to 0.2981 p.u. during the fault condition before gradually recovering to 0.92853 p.u. after fault clearance as shown in figure 4.

These results indicate poor transient stability performance and weak damping capability in the existing BEDC network.

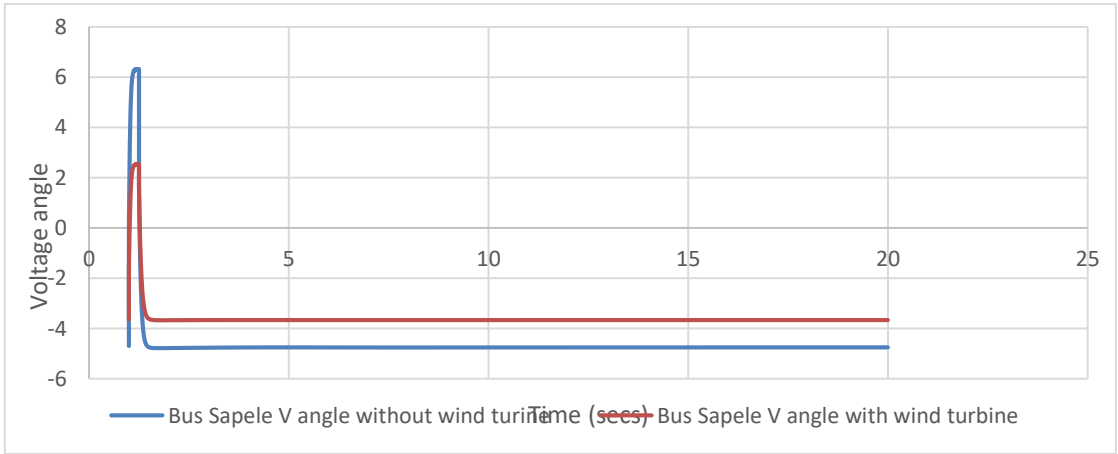

Figure 5: A plot of the voltage angle against time with the connection of the Wind Turbine

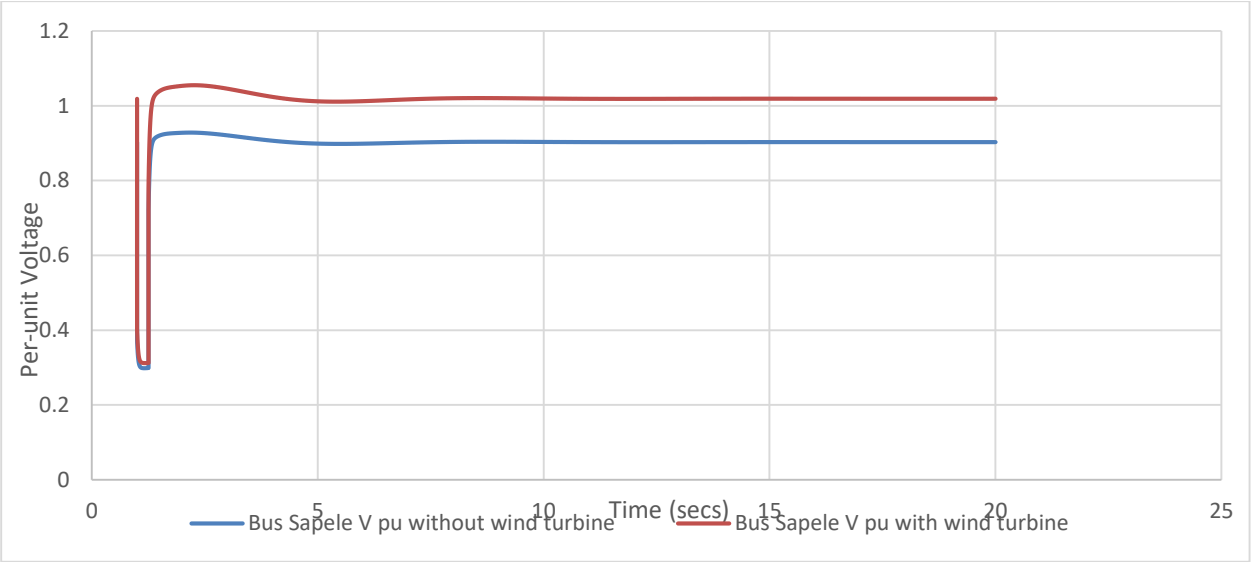

Figure 6: A plot of the voltage per-unit against time with the connection of the Wind Turbine

After integrating the wind turbine into the BEDC network, significant improvements were observed in system voltage stability and transient response.
The maximum voltage angle reduced from 6.32887° to 2.53556°, while the minimum voltage angle improved from −4.77947° to −3.67588° as shown in figure 5.
Furthermore, the system stabilization time reduced drastically from 4.7503 seconds to 2.191762 seconds.
The minimum per-unit voltage during the fault also improved from 0.2981 p.u. to 0.31153 p.u., while the maximum steady-state voltage increased from 1.05489 pu at about 2.25 seconds. but it eventually stabilized at approximately 1.01876 pu as shown in figure 6.
These improvements indicate that the wind turbine provided additional reactive power support and enhanced damping characteristics during the fault condition.

3.1 Discussion of Results

The results demonstrate that wind-turbine integration improved the voltage-stability performance of the modeled BEDC network. The increase in minimum fault voltage from 0.2981 p.u. to 0.31153 p.u. is consistent with the voltage-support benefits reported by Adetokun et al. (2020) and Adetokun and Muriithi (2021), who found that appropriately integrated DFIG-based wind generation can improve voltage margins in weak grids.
The reduction in voltage-angle oscillations and the decrease in stabilization time from 4.7503 s to 2.191762 s indicate improved damping and faster post-fault recovery. This agrees with Tina et al. (2022), who showed that appropriate wind-system support can improve transient performance,
The improved per-unit voltage profile also suggests stronger voltage support during and after the disturbance. However, the improvement observed in the BEDC case should be interpreted in relation to the modeled turbine characteristics, connection point, fault location, and control assumptions, because these factors can materially change system response.
Overall, the BEDC results extend the existing literature by providing a localized Nigerian distribution-network case in which both voltage magnitude and voltage-angle recovery are compared quantitatively before and after wind-turbine integration. The findings support the view that renewable generation can strengthen a weak network when its connection are appropriately coordinated, while also reinforcing the need for case-specific transient studies before large-scale deployment.

4. Conclusion

This study investigated the voltage stability of a grid-connected wind turbine on the BEDC network using Newton–Raphson load flow analysis and transient simulation techniques.
Simulation results revealed that integrating wind energy into the BEDC network significantly improved voltage stability and transient response during fault conditions.
The system stabilization time reduced from 4.7503 seconds to 2.191762 seconds after wind turbine integration. Furthermore, voltage oscillations reduced considerably, and the network demonstrated improved damping characteristics.
The findings confirm that wind energy integration can improve power system reliability, reduce voltage instability, and enhance the performance of weak distribution networks such as BEDC

5.0 Recommendation

Given the ability of the test network to stabilize with the addition of wind turbine, we recommend that wind turbine can as well be used to support existing power system network in Nigeria. Given its sustainable nature, it will help increase Nigerian green energy contribution.

Declaration of Generative AI and AI-assisted technologies in the writing process

During the preparation of this work the author(s) used ChatGPT in order to correct grammatical errors as well as generate graphical abstract. After using this tool/service, the author(s) reviewed and edited the content as needed and take(s) full responsibility for the content of the publication.

References

Akuru, U. B., Onukwube, I. E., Okoro, O. I., & Obe, E. S. (2017). Towards 100% renewable energy in Nigeria. Renewable and Sustainable Energy Reviews, 71, 943–953. https://doi.org/10.1016/j.rser.2016.12.123

Flynn, D., Rather, Z., Ardal, A., D'Arco, S., Hansen, A. D., Cutululis, N. A., Sørensen, P. E., Estanqueiro, A., Gomez, E., Menemenlis, N., Smith, C., & Wang, Y. (2017). Technical impacts of high penetration levels of wind power on power system stability. Wiley Interdisciplinary Reviews: Energy and Environment, 6(2), e216. https://doi.org/10.1002/wene.216

Xia, S., Zhang, Q., Hussain, S. T., Hong, B., & Zou, W. (2018). Impacts of integration of wind farms on power system transient stability. Applied Sciences, 8(8), 1289. https://doi.org/10.3390/app8081289

Adetokun, B. B., Muriithi, C. M., & Ojo, J. O. (2020). Voltage stability assessment and enhancement of power grid with increasing wind energy penetration. International Journal of Electrical Power & Energy Systems, 120, 105988. https://doi.org/10.1016/j.ijepes.2020.105988

Adetokun, B. B., & Muriithi, C. M. (2021). Impact of integrating large-scale DFIG-based wind energy conversion system on the voltage stability of weak national grids: A case study of the Nigerian power grid. Energy Reports, 7, 654–666. https://doi.org/10.1016/j.egyr.2021.01.025

Hu, Q., Xiong, Y., Liu, C., Wang, G., & Ma, Y. (2022). Transient stability analysis of direct drive wind turbine in DC-link voltage control timescale during grid fault. Processes, 10(4), 774. https://doi.org/10.3390/pr10040774

Tina, G. M., Maione, G., & Licciardello, S. (2022). Evaluation of technical solutions to improve transient stability in power systems with wind power generation. Energies, 15(19), 7055. https://doi.org/10.3390/en15197055

Shabani, H. R., Hajizadeh, A., Kalantar, M., Lashgari, M., & Nozarian, M. (2023). Transient stability analysis of DFIG-based wind farm-integrated power system considering gearbox ratio and reactive power control. Electrical Engineering, 105, 3719–3735. https://doi.org/10.1007/s00202-023-01906-3

Verma, N., Kumar, N., Gupta, S., Malik, H., & García Márquez, F. P. (2023). Review of sub-synchronous interaction in wind integrated power systems: Classification, challenges, and mitigation techniques. Protection and Control of Modern Power Systems, 8, 17. https://doi.org/10.1186/s41601-023-00291-0

Malik, F. H., Khan, M. W., Rahman, T. U., Ehtisham, M., Faheem, M., Haider, Z. M., & Lehtonen, M. (2024). A comprehensive review on voltage stability in wind-integrated power systems. Energies, 17(3), 644. https://doi.org/10.3390/en17030644.